Geophysical Research Letters

RESEARCH LETTER
10.1029/2022GL099681

Key Points:

- We present an entropy-based metric, Entropic Braiding Index (*eBI*), that quantifies braiding intensity by providing the effective number of channels per cross-section
- *eBI* is more robust than previous metrics to changes in resolution by accounting for channel diversity in terms of scale (e.g., water discharge)
- *eBI* can differentiate between braided and anastomosed systems and assess river cross-sectional stability in response to seasonal flooding

Correspondence to:
A. Tejedor,
alejt.tejedor@gmail.com

Citation:
Tejedor, A., Schwenk, J., Kleinhans, M., Limaye, A. B., Vulis, L., Carling, P., et al. (2022). The entropic Braiding Index (*eBI*): A robust metric to account for the diversity of channel scales in multi-thread rivers. *Geophysical Research Letters*, *49*, e2022GL099681. https://doi.org/10.1029/2022GL099681

Received 25 MAY 2022
Accepted 2 AUG 2022

The Entropic Braiding Index (*eBI*): A Robust Metric to Account for the Diversity of Channel Scales in Multi-Thread Rivers

Alejandro Tejedor[1,2], Jon Schwenk[3], Maarten Kleinhans[4], Ajay B. Limaye[5], Lawrence Vulis[2], Paul Carling[6], Holger Kantz[7], and Efi Foufoula-Georgiou[2,8]

[1]Department of Science and Engineering, Sorbonne University Abu Dhabi, Abu Dhabi, United Arab Emirates, [2]Department of Civil and Environmental Engineering, University of California, Irvine, CA, USA, [3]Los Alamos National Laboratory, Division of Earth and Environmental Sciences, Los Alamos, NM, USA, [4]Faculty of Geosciences, Utrecht University, Utrecht, The Netherlands, [5]Department of Environmental Sciences, University of Virginia, Charlottesville, VA, USA, [6]Geography and Environmental Science, University of Southampton, Southampton, UK, [7]Max Planck Institute for the Physics of Complex Systems, Dresden, Germany, [8]Department of Earth System Science, University of California, Irvine, CA, USA

Abstract The Braiding Index (*BI*), defined as the average count of intercepted channels per cross-section, is a widely used metric for characterizing multi-thread river systems. However, it does not account for the diversity of channels (e.g., in terms of water discharge) within different cross-sections, omitting important information related to system complexity. Here we present a modification of *BI,* the Entropic Braiding Index (*eBI*), which augments the information content in *BI* by using Shannon Entropy to encode the diversity of channels in each cross section. *eBI* is interpreted as the number of "effective channels" per cross-section, allowing a direct comparison with the traditional *BI*. We demonstrate the potential of the ratio *BI/eBI* to quantify channel disparity, differentiate types of multi-thread systems (braided vs. anastomosed), and assess the effect of discharge variability, such as seasonal flooding, on river cross-section stability.

Plain Language Summary Multi-thread rivers display astonishingly complex patterns with multiple channels splitting and joining to form intricate networks. Multi-thread rivers are often highly dynamic, and seasonal flooding can trigger significant channel reorganization. Understanding multi-thread systems and their dynamics relies on our capacity to characterize them. However, the most widely used metric to analyze multi-thread systems—the Braiding Index (*BI*)—is just the average count of channels per cross-section. *BI* is blind to differences in channel scale (water discharge, width) and, thus, *BI* is very sensitive to observational resolution—higher resolution would reveal smaller channels, often orders of magnitude smaller than the largest channels. Here we propose a modification of the *BI* using concepts of entropy - the entropic *BI*, *eBI* - which encodes not only the channel count but also the heterogeneity of channels in terms of scale (flow, channel width, or any other relevant property) within cross-sections. We demonstrate that *eBI* is a robust and suitable metric to characterize multi-thread systems, differentiate between braided and anastomosed systems, and provide information about river cross-section stability to forcing, for example, seasonal flooding.

1. Introduction

Channels routing water and sediment across the Earth's surface exhibit different configurations, ranging from single-thread (straight and meandering) to multi-thread (braided, anabranched and anastomosed) patterns (Eaton et al., 2010; Huang & Nanson, 2007; Leopold & Wolman, 1957). Our ever-increasing capacity to observe Earth's surface via remote sensing allows us not only to characterize these patterns globally but also witness their dynamic nature by using the archive of nearly 50 years of satellite imagery (e.g., Landsat).

Braided rivers exhibit intricate and complex patterns while being highly dynamic, wherein their channel-bar complex can be substantially reconfigured due to discharge variability, including seasonal flooding. Although significant strides have been made to better characterize and understand the multi-scale dynamics of these complex systems, for example, using space-time renormalization theory (e.g., Foufoula-Georgiou & Sapozhnikov, 2001; Sapozhnikov & Foufoula-Georgiou, 1999; Sapozhnikov et al., 1998) or network theory (e.g., Marra et al., 2014), the most commonly adopted indices to quantify the *braiding intensity* of a river (Egozi & Ashmore, 2008) focus on bar properties, channel count, or channel sinuosity. Particularly, as the defining characteristic of a braided river is its multiple channel threads, the most commonly applied metric of a braided river—the Braiding Index (*BI*)—captures this essential characteristic by counting the number of channel threads per river cross-section (e.g., Egozi & Ashmore, 2009; Kleinhans & van den Berg, 2011; Limaye, 2017; Limaye et al., 2018; Meshkova & Carling, 2013; Nicholas, 2013). However, despite its wide use, this index has important limitations: (a) *It is a simple count*—and is therefore insensitive to the differences in water discharge and sediment flux between adjacent threads, which can vary by orders of magnitude (see Figure 1b for an example of channel heterogeneity in a cross-section). (b) *It is sensitive to resolution*—as the resolution is increased, smaller channels can be observed, varying the value of *BI* abruptly. This resolution dependence is problematic because advances in satellite imaging in recent years have created an historical archive of data that spans a wide range in resolution. (c) *It is sensitive to water level*—the channel count is highly sensitive to flow discharge and stage, increasing the number of flooded channels in intermediate discharge but decreasing the number in extreme floods that submerges the bars. These limitations in this characteristic metric of braided rivers hinder our ability to understand the complexity of these systems relative to the underlying relevant physical variables, as well as to compare geometric and dynamic patterns across systems (Carling et al., 2014).

Here, we propose a new metric for braiding intensity called the Entropic *BI*, *eBI*, which addresses the crucial limitations noted above for *BI*. The *eBI* is more robust to changes in resolution and water level, and acknowledges the water discharge heterogeneity of the channels co-existing in a given cross-section, while keeping some of the key properties of the traditional *BI*, that is, its simplicity, interpretability, and relevance to the essential multi-thread nature of braided rivers. As we demonstrate in this work, *eBI* can be interpreted as the effective number of channels per cross-section. The definition of effective number of channels is rooted in a probabilistic Lagrangian view of transport, the uncertainty of which is characterized by Shannon Entropy (Shannon, 1948), resulting in a metric that suitably integrates the information of the channel count and the relative size of the channels (e.g., in terms of water discharge) per cross-section.

In what follows, we first briefly introduce the concept of Shannon Entropy as a measure of uncertainty, which is the basis for defining the *eBI*. We continue with a comparison of *BI* and *eBI* through some illustrative synthetic examples and for a field case, showcasing the ability of *eBI* to provide an effective count of channels per cross-section that acknowledges information about channel disparity. Finally, via analysis of a wide range of numerically simulated multi-thread rivers with varying sediment size, and with and without vegetation we demonstrate the potential of *eBI* and the ratio *BI/eBI*, to differentiate between braided and anastomosed systems, and to assess river cross-section stability (in terms of channel persistence) in response to streamflow variability, including seasonal flooding.

2. Shannon Entropy

The cornerstone of information theory is Shannon Entropy, which quantifies the uncertainty in the outcome of a stochastic process (e.g., flipping a coin or rolling a die). In other words, Shannon Entropy quantifies the amount of information needed to describe (on average) the resulting outcome of a stochastic process (Cover & Thomas, 2006). Uncertainty can be derived intuitively from the notions of probability and surprise. For a given discrete stochastic process $\{x_i\}$, such as rolling a die, with a specified probability distribution of outcomes, for example, $\{p_1 = 5/6; p_2 = 1/6\}$ for a six-sided die with five sides labelled with number one and one side labelled with number two. Intuitively, the occurrence of rolling a one is less surprising than rolling a two. Mathematically, the surprise associated with a given outcome x_i can be expressed as $-\log(p_i)$, which matches our intuitive notion of surprise: the occurrence of outcome with probability one, $p_i = 1$ (e.g., rolling a number smaller than three in the die described above), produces zero surprise since $-\log(1) = 0$; while the occurrence of an impossible outcome, $p_i = 0$ (e.g., rolling a three with the die described above), would produce an infinite surprise since $-\log(0) = \infty$. The uncertainty of a particular outcome, h_i, is defined as the surprise that this outcome produces, $-\log(p_i)$, times the probability of its occurrence p_i. Therefore, the uncertainty associated with either a completely certain event ($p_i = 1$) or an impossible one ($p_i = 0$) is zero. The uncertainty, or Shannon Entropy H, associated with a discrete stochastic process, with N possible outcomes with probabilities $\{p_1, p_2, \ldots, p_i, \ldots, p_N\}$, is equal to the sum of the uncertainties introduced by each outcome x_i:

$$H = \sum_{i=1}^{N} h_i = -\sum_{i=1}^{N} p_i \log_2 p_i \qquad (1)$$

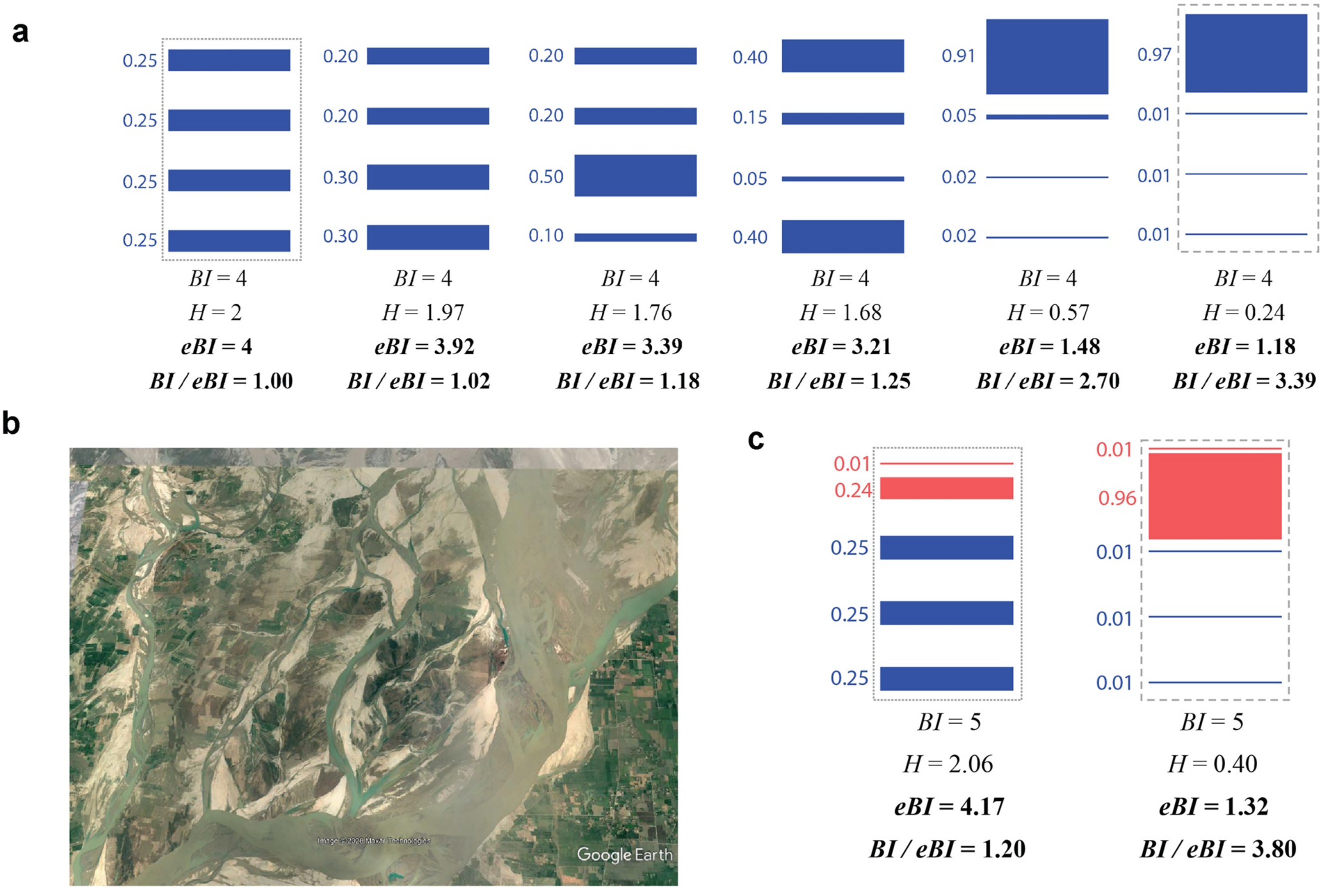

Figure 1. Illustration of the difference between braiding index (*BI*) and entropic braiding index (*eBI*). (a) *Channel heterogeneity*. The illustration shows a schematic of six river cross-sections (columns), each containing 4 channels represented by blue bands. The width of each band is considered here as a proxy for the relative discharge for each channel (indicated by the number to the left of each band). While *BI* is four for all the six configurations, the values of Shannon entropy (*H*) decrease from left (maximum value for 4 channels) to right. The *eBI* computed as 2^H is also displayed for each configuration. *eBI* can be interpreted as the equivalent number of equally sized channels characterized by the same value of *H*. The value of *eBI* matches our intuition as an integrative measure of the channel count while accounting the heterogeneity in channel scale. Finally, the *BI/eBI* ratio, which quantifies the heterogeneity in the flux distribution conveyed by the different channels co-existing in a cross-section, is displayed. (b) *Field Example*. Section of the Indus River illustrating the diversity of channels (in terms of width) which co-exist in river cross-sections. (c) *Effect of resolution*. It displays two synthetic scenarios wherein we illustrate the change in *BI* and *eBI* when resolution is increased, and as a result the number of channels visualized changes. The left (right) example corresponds to the example highlighted with a dotted (dashed) rectangle in panel (a), where under an increased resolution scenario, the top channel (top blue band in a) is resolved into two channels (two red bands in c). The new resolution scenario changes the value of *BI* from 4 to 5 for both configurations, while *eBI* changes from 4 to 4.17 for the left cross-section and from 1.18 to 1.32 for the right cross-section, indicating a more robust and relevant behavior of *eBI* in comparison with *BI*.

Note that traditionally the logarithm used is in base 2, which is reminiscent of the origin of Shannon Entropy within the field of signal processing, where the $\log_2$ leads to the interpretation of uncertainty in terms of bits of information that need to be transmitted on average to determine a given outcome. In other words, *H* is the minimum number of yes/no questions that are needed to determine, on average, the outcome of the stochastic process.

H is maximal ($H_{max}(N)$) when all the *N* possible outcomes have the same probability of occurrence $1/N$, for example, rolling a fair six-faced die with a different number on each face and each having a probability of occurrence 1/6 (Cover & Thomas, 2006). Note that $H_{max}(N)$ scales logarithmically with the number of possible outcomes *N*.

$$H_{\max}(N) = \sum_{i=1}^{N} h_i = -\sum_{i=1}^{N} \frac{1}{N}\log_2\frac{1}{N} = -N\left(\frac{1}{N}\log_2\frac{1}{N}\right) = \log_2 N \tag{2}$$

Shannon Entropy, and derived quantities based on this concept, have been widely used in different applications in hydrology and geomorphology (e.g., Feng et al., 2013; Fiorentino et al., 1993; Gong et al., 2013; Goodwell &

Kumar, 2017; Nearing & Gupta, 2015; Porporato & Rodriguez-Iturbe, 2013; Ranjbar & Singh, 2020; Ruddell & Kumar, 2009a, 2009b; Singh, 1997; Tejedor et al., 2017).

3. Defining and Interpreting the Entropic Braiding Index, *eBI*

In this section we utilize a series of examples to illustrate the applicability of Shannon entropy to characterize multi-thread rivers, introducing the concept of the entropic *BI*, *eBI*, and pointing out some of the advantages of the new metric when compared with the traditional *BI*. Particularly, Figure 1a shows a synthetic example of six river cross-sections, each of them containing four channel threads, and therefore characterized by $BI = 4$. This example highlights the fact that the characterization of a multi-thread river via *BI* is quite coarse because the simple channel count ignores the relative size of the co-existing channels (e.g., in terms of water discharge) at the cross-section.

We propose using Shannon entropy as a more robust and meaningful characterization of the cross-sectional properties of multi-thread rivers. In this case, the problem may be reformulated from the point of view of probabilistic Lagrangian transport. A tracer injected upstream of the multi-thread channel has a certain probability to eventually go through each of the different channel threads at a given cross-section. Each cross-section of the full river can be abstracted as a stochastic process with a number of outcomes equal to the number of channel threads observed at that cross-section (i.e., four for all the cases shown in Figure 1a). The probability of each outcome is given by the relative flow of the corresponding channel thread with respect to the total flow conveyed by all channels at that cross-section. Thus, the Shannon entropy H associated to each cross-section, can be computed as follows

$$H = \sum_{i=1}^{N} h_i = -\sum_{i=1}^{N} \frac{q_i}{Q} \log_2 \frac{q_i}{Q} \tag{3}$$

where q_i is the flow going through channel i in that cross-section, and $Q = \sum q_i$ is the total water discharge going through that cross-section (Figure 1a shows the ratio q_i/Q, which can be interpreted as probability, to the left of each band). The value of H is the highest (given a channel count) for systems consisting of channel threads carrying equal flow (leftmost column in Figure 1a) because this case maximizes the uncertainty for the path of a tracer particle. In contrast, systems dominated by a single channel are characterized by low values of H due to low path uncertainty (e.g., rightmost column in Figure 1a). Figure 1c also shows the robustness of this metric under different resolutions. In particular, Figure 1c presents a synthetic scenario wherein, by increasing the resolution, an apparently singular channel thread in Figure 1a is resolved as two different channels at the finer resolution (the example uses the two endmembers from Figure 1a—the left- and rightmost columns—where the top channel is resolved as two different channels in Figure 1c under higher resolution). While the traditional *BI* jumps from four to five under the increasing resolution scenario, the change in the value of H (from 2 to 2.06) reflects more suitably the addition of a very narrow channel with minimal flow.

Although H is a suitable metric to directly characterize multi-thread systems, unlike the traditional *BI*, its value is not directly interpretable in terms of a geomorphic feature. More importantly, it is not straightforward to compare H with more widely used metrics such as *BI*. To overcome these issues, we propose to define the entropic *BI*, *eBI*, as

$$eBI = 2^H \tag{4}$$

eBI is an increasing function of H, and according to Equation 2, can be interpreted as the equivalent number of channels that a multi-thread system consisting of identical (in terms of water discharge) channels would have. Thus, *eBI* is interpreted here as an *effective channel count* that integrates the information relative to the number of channels together with the relative importance of those channels in terms of water discharge. Note that for a system where all the channels exhibit equal discharge, that is, $q_i = Q/N\ \forall i$, the *eBI* achieves the same value as the traditional *BI*. As shown in Figure 1a, *eBI* captures important information elusive to *BI*, while offering an interpretable value that intuitively reflects the number of effective channels occurring per cross-section. Furthermore, the ratio *BI/eBI* quantifies the heterogeneity of flux distribution in the cross-section and varies from 1, for cases with equal discharge in co-existing channels, and tends to *BI* for cases with one dominant channel (see Figure 1a). Finally, Figure 1c shows that, under an increase in resolution, *eBI* is much more robust than the traditional *BI*.

10.1029/2022GL099681

4. Examples of *eBI* in Action

In this section, we first present a field case comparison of the traditional *BI* and the new *eBI* to demonstrate the robustness of *eBI* to resolution and its ability to characterize channel heterogeneity. We then examine different types of multi-thread rivers in numerical simulations, where several variables such as water discharge, vegetation, or sediment size were controlled and demonstrate that the ratio *BI/eBI* is able to differentiate between different types of multi-thread rivers, such as braided versus anastomosed. Finally, we ask the question as to whether *BI/eBI* can shed light on the dynamics and stability of cross-sections, in response to perturbations. In particular, we examine whether cross-sections characterized by a large value of *BI/eBI* (heterogeneous cross-sections in terms of channel thread discharge) are more prone to be reconfigured by streamflow variability or seasonal flooding.

For simplicity and consistency in our analysis, we have used channel width as a proxy for the water discharge partition both for the field case study and the numerically simulated systems (e.g., see Ashmore, 2007; Dong et al., 2020; Fahnestock, 1963; Gaurav et al., 2015; Hariharan et al., 2022). We note however that our framework is applicable for any system-specific nonlinear function of discharge to width, if such a relationship is available. Using width as a surrogate for discharge, Equation 2 becomes

$$H = \sum_{i=1}^{N} h_i = -\sum_{i=1}^{N} \frac{w_i}{W} \log_2 \frac{w_i}{W} \tag{5}$$

where for each cross-section: N is the number of channels, w_i is the width of its ith channel, and $W = \sum_{i=1}^{N} w_i$ is the total wet width (note the ratio $\frac{w_i}{W}$ can be interpreted as a probability). With this definition of H, *eBI* is computed as 2^H.

4.1. Using *eBI* to Characterize Cross-Section Channel Diversity/Heterogeneity

To demonstrate the ability of *eBI* to quantify channel diversity, we analyzed a braided section of the Indus River at mean annual discharge. We used a 30 m spatial resolution mask from the Global River Widths from Landsat database (Allen & Pavelsky, 2018) with the Python package *RivGraph* (Schwenk et al., 2020; Schwenk & Hariharan, 2021) to automatically obtain channel counts and widths, generate transects, and directly compute *BI* and *eBI* across each transect.

Figure 2a shows the locations of several cross sections whose corresponding measurements of braiding intensity are shown in Figures 2b–2d. This comparison showcases the key properties of *eBI* with regard to the traditional *BI*: (a) *eBI is more informative and robust*—*eBI* provides information about the changes in the planform geometry of the multi-thread system in terms of distribution of water discharge among the active channels, while *BI* is insensitive to these properties. For example, Figure 2c shows a transect at which the traditional *BI* is more than double the *eBI* due to the presence of very small channels (relative to the widest one). At the same time, *eBI* is more robust to changes in resolution, as illustrated with the schematic in Figure 1c. (b) *BI is an upper bound for eBI*—We note that by definition, *eBI* is equal to *BI* when all the channels co-existing in a given cross-section have equal probability of receiving fluxes from upstream (i.e., in this analysis in terms of width). Any other configuration results in a value of *eBI* lower than *BI*. Moreover, note that it is possible that two cross-sections with a different *BI* could be characterized by the same (or very similar) number of effective channels as defined by *eBI*. (c) *BI/eBI quantifies channel heterogeneity*—From the mathematical point of view, the value of *eBI* accounts both for the number of channels and their relative size (in terms of water discharge or width), providing a number of effective channels, while *BI* solely accounts for the channel count. *BI/eBI* (Figure 2b), far for being random, quantifies the heterogeneity of the channels present in the different cross-sections (the more variable the channels are in terms of width, the higher the ratio of the two indices). Note that the ratio *BI/eBI* is able to differentiate cross-sections characterized by a similar number of effective channels (*eBI*), but different *BI*.

The *eBI* features discussed above significantly improve the characterization of multi-thread systems in contrast to *BI* as they provide additional valuable information about the whole system, while being simple to compute from local (cross-sectional) information only, as opposed to other whole-network metrics based on graph theory (e.g., Tejedor et al., 2015a, 2015b, 2016, 2017, 2018; Marra et al., 2014).

10.1029/2022GL099681

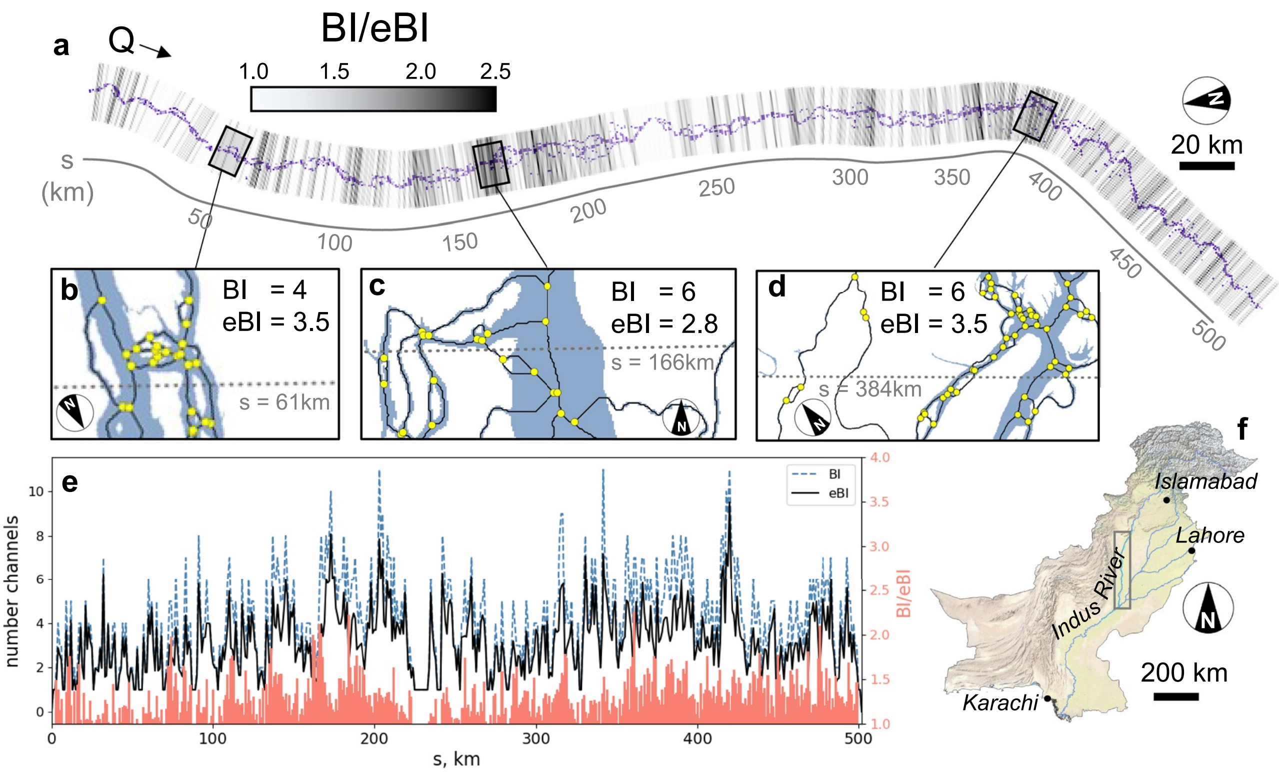

Figure 2. Indus River. (a) *The Indus River* (see panel f for reference) channel structure was extracted using RivGraph on the Global River Widths from Landsat product (Allen & Pavelsky, 2018). The cross-sections used for our analysis are marked with segments colored according to the value of the ratio *BI/eBI*. (b-c) *Channel heterogeneity*. Three different cross-sections (rotated for illustration purposes) corresponding to the annotated streamwise distance *s* are depicted in detail showing the channel network structure. These panels provide evidence of the variability in width of the co-existing channels per cross-section. (e) *Braiding intensity*. The values of Braiding Index (*BI*), entropic braiding index (*eBI*) are shown for each of the transects shown in (a). The ratio *BI/eBI* is also displayed in pink, providing a quantitative measure of the diversity of channel widths along the river.

4.2. Using *eBI* to Interpret the Effects of Streamflow Variability on Channel Diversity and Differentiate Types of Multi-Thread River Systems

In the interest of characterizing systems under different hydrologic conditions but in a controlled environment and for long time spans, we present here the results corresponding to the analysis of different multi-thread systems obtained from numerical simulations. Particularly, we utilized some of the model outputs presented by Kleinhans et al. (2018) for the River Allier (France), which were obtained using the depth-averaged version of Delft3D, with the vegetation module developed by van Oorschot et al. (2017). Depending on the local abundance of mud in the bed surface layer, sediment transport was either modeled by a transport capacity predictor for the bed sediment or by excess shear stress relations for sedimentation and erosion of cohesive sediment transported by advection-diffusion (see Braat et al., 2017 for detailed formulations). From all the runs presented in Kleinhans et al. (2018), we chose five runs (see Figure 3b for a table containing the key parameters) that offered a broad range of variability from the geomorphologic point of view, ranging from an anastomosed system with more stable banks to very active braided systems.

Each of the numerical experiments analyzed herein was set up with the boundary conditions corresponding to the River Allier and were initialized with a set of symmetrical bends (for more details see Kleinhans et al., 2018). For each run, the system was forced by a 300 year (except for Run 5 with a 150 year) time series of water discharge between 50 and 400 m^3s^{-1}, randomly sampled from five typical flood hydrographs. Then, for each run, we extracted two water masks (low and high flow) per year of the simulation by simply thresholding on water depth. Each of those water masks was analyzed using *RivGraph* to obtain the channel count and channel widths per cross-section (here as in the case of observational data, we use channel width as a proxy for discharge for consistency). In our analysis, we discarded the first 75 years for each simulation to avoid the effects of initial conditions.

a

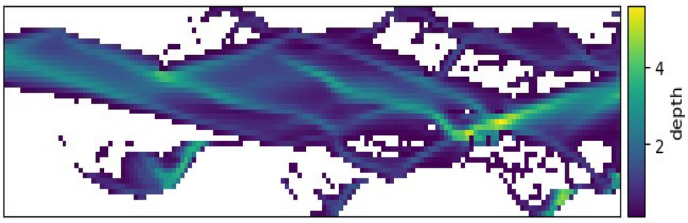

b

Run	Vegetation	Mud Supply (gm^3)	Critical shear (Nm^2)
1	Yes	0	n.a.
2	Yes	20	0.2
3	No	20	0.2
4	No	0	n.a.
5	Yes	500	0.5

c

d

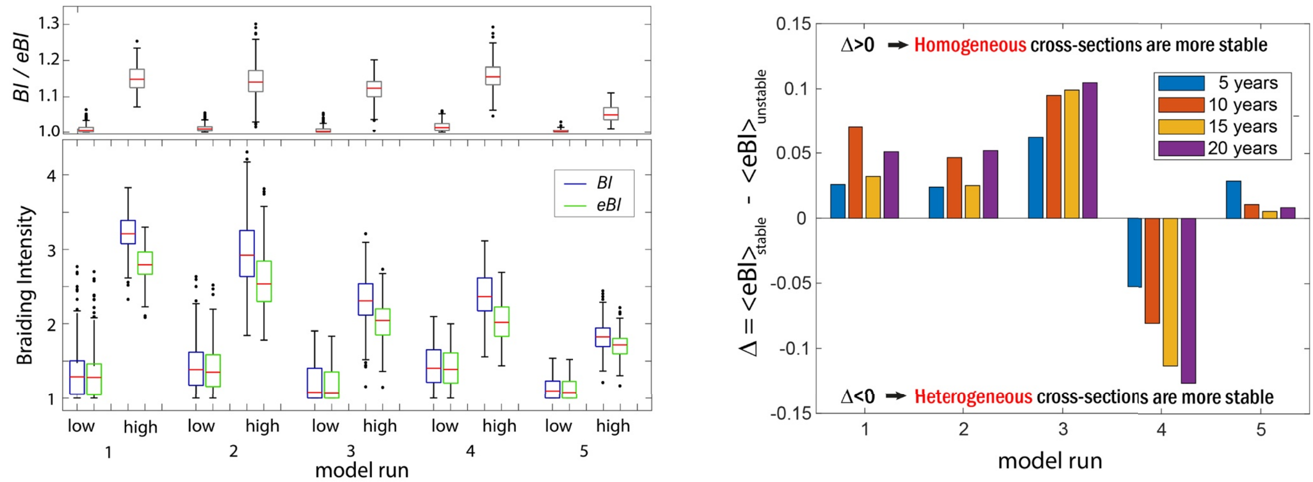

Figure 3. Numerically simulated multi-threaded channel. (a) *Model output*. Illustration of model output in terms of water depth field. (b) *Model runs*. Table containing the key parameters of the different model runs selected from Kleinhans et al. (2018). (c) *Braiding Intensity*. Comparison of the range of the values of Braiding Index (*BI* – dark blue) entropic braiding index (*eBI* – light green) and *BI/eBI* (top panel) for each model run and for low and high levels of discharge. For each box plot, the lower and upper limit of the box represent the first (Q_1) and third (Q_3) quartiles respectively, while the horizontal line within the box (red) corresponds to the median. The whiskers extent 1.5 times the interquartile range (Q_3–Q_1) capped to the maximum/minimum value of the data set. (d) *Cross-section stability*. Δ, that is, the mean difference of *eBI* for *k*-year 2-channel stable and *k*-year 2-channel unstable cross-sections (k = 5, 10, 15 and 20 years) for each model run are displayed. Positive (negative) values of Δ indicate that stable (unstable) cross-sections exhibit more (less) homogeneous cross-sections in terms of channel widths than unstable (stable) cross-sections, and therefore a larger (smaller) number of effective channels. Our analysis shows that stable cross-sections consist of more homogeneous channels in the presence of vegetation and/or cohesive sediment, while channel disparity characterizes stable cross-sections for the run that have a sandy sediment supply and lack vegetation.

For similar reasons, 30% of the spatial domain (15% from the upstream and 15% from the downstream boundaries) was discarded to avoid spurious effects introduced by the upstream and downstream boundary conditions.

For each run, multi-thread patterns of different complexity and degree of dynamism emerged (See Figure 3a for an instance of one of the simulations for illustration purposes). The analysis of these systems according to the *eBI*, as well as its comparison with the traditional *BI*, yields the following important results as revealed from Figure 3c: (a) *Regarding low* versus *high flow conditions*: The value of *eBI* for low flow conditions is significantly lower than for those corresponding to high flow conditions. This result is also reflected in the analysis of the system via the *BI*, which documents the activation of fewer channels during the low flow conditions when compared with the higher discharge. However, some key information is revealed by the *eBI* when compared with *BI*: channels co-existing in the different cross-sections at the low discharge regime are more uniform in terms of widths as captured by the small value of *BI/eBI*, while at higher discharge levels the width disparity among channels increases as a consequence of the activation of small channels, which can be an order of magnitude smaller than the dominant channels conveying most of the water and sediment. (b) *Braided* versus *Anastomosed systems*: From all the model runs analyzed, run 5 corresponds to an anastomosed system, while the other four runs could be classified as braided systems. From our analysis, we can conclude that the anastomosed system develops channels less diverse in width compared with braided river systems at high flow regimes, as is evident from the significantly smaller values of *BI/eBI* for the anastomosed system (run 5), in comparison with the braided rivers (runs 1– 4).

4.3. Using *eBI* to Assess Cross-Section Stability in Response to Streamflow Variabiliy or Seasonal Flooding

Given the interest in identifying possible emergent behavior of these complex systems in response to perturbations or future forcing, we posed the following question: does channel heterogeneity in a cross-section (in terms of the discharge carried by each channel) provide information about the potential (in)stability of the system in terms of maintaining the number of threads in that specific cross section? Or, in other words, are cross-sections characterized by a higher channel-width disparity less stable to perturbations (e.g., seasonal flooding) than those cross-sections of more uniform channels in terms of widths? To shed light on this question, we performed the following analysis. For each model run, we monitored the temporal evolution of the 74 cross-sections in which we discretized the spatial domain. Specifically, we analyzed the system evolution retrospectively, documenting every time that a cross-section was reconfigured in terms of experiencing a change in its number of co-existing channels. For those reconfigurations, we recorded the time, the cross-section location, the new number of co-existing channels, and their persistence, that is, the number of years (in model time) for which the new number of channels was sustained in that cross-section. Thus, we define a "k-year, n-channel stable cross-section" as a cross-section that was able to maintain n-channels for a period of k years or more. Given this definition, the question that we want to address is whether k-year, n-channel stable cross-sections are characterized by a different degree of channel similarity (in terms of width) than that corresponding to k-year n-channel *unstable* cross-sections (note that a k-year n-channel unstable cross-section is defined as a cross-section that is not able to sustain n channels during k-consecutive years). In other words, are systems with less diverse channels exhibiting more or less stability (persistence) in maintaining those channels over long time periods? Note that because in our analysis we were controlling the number of channels per cross-section, n, channel similarity is directly quantified by the number of effective channels, *eBI* (i.e., the more homogeneous the channels are in terms of width, the closer the number of effective channels is to n). Given the spatiotemporal domain offered by the model runs as well as the characteristics of the model parameters, we present our analysis only for k-year 2-channel (un-)stable cross-sections (for $k = 5,10,15$ and 20 years) as for $n > 2$ the number of occurrences is too limited to show statistically robust results. Particularly, for each model run and threshold of temporal stability ($k = 5,10$, 15 and 20 years), we computed the difference, Δ, between the mean *eBI* for stable and unstable cross-sections:

$$\Delta = \langle eBI \rangle_{k-\text{year, 2-channel stable cross-section}} - \langle eBI \rangle_{k-\text{year, 2-channel unstable cross-section}} \tag{6}$$

where a system characterized by $\Delta > 0$ exhibits stable cross-sections with a higher number of effective channels, that is, stable cross-sections are on average more homogeneous in terms of channel widths; while $\Delta < 0$ corresponds to systems for which stable cross-sections on average exhibit a higher channel width disparity (heterogeneous cross-sections), and therefore, smaller *eBI*.

The results of our analysis (see Figure 3d) show three different scenarios: (a) *Runs 1, 2, and 3*: Stable cross-sections are characterized by more uniform channels than unstable cross-sections. The three runs showing this behavior have in common different mechanisms of channel stability (sediment cohesion and/or vegetation). In those cases, co-existing channels of similar size are able to create channel structures in the floodplain that are more stable given variations in water discharge, while co-existing relatively smaller channels are less likely to generate positive feedbacks with vegetation and/or establish stable banks (cohesive sediment) maintaining their structure and geometry during more extended periods of time. (b) *Run 4—Only Sand*: Cross-section stability is characterized by a larger channel disparity in comparison with the unstable counterparts. The higher channel mobility in unstable systems allows the co-existence of channels of different sizes, although with large variability in the nature of the co-existing channels in terms of their relative water discharge, as shown by negative values of Δ. (c) *Run 5 -Anastomosed system*: In this case, it appears that channel width disparity is not a good explanatory variable of cross-section stability, because both stable and unstable cross-sections yield values of Δ close to zero. We attribute this outcome to the fact that the channels present in anastomosed systems are consistently more uniform across the spatio-temporal domain of the run, as shown and discussed before (see Figure 2c) and therefore distinguishing between stable and unstable cross-sections might require a more detailed study.

Although the previous analysis is by no means a systematic analysis of cross-section channel stability, it nevertheless presents evidence of the potential of the new metric introduced here, *eBI*, to not only characterize the static patterns of multi-thread systems but also to serve as a tool for studying system response to forcing in terms of the dynamic behavior and stability of channels.

5. Conclusions and Perspectives

Multi-thread fluvial systems are some of the most astonishing and intricate patterns observed on the Earth's surface. Their complexity and dynamic nature hinder their characterization and our ability to assess their evolution and response to future forcings. Many metrics have been proposed to characterize those systems (e.g., channel count, channel link length, island geometry, etc.) but the *BI* has been widely used as it is a simple measure of the number of channels intercepted at a section, averaged over several cross sections of the system. By definition, *BI* does not account for channel heterogeneity, that is, all channels are counted equally no matter how different they are in terms of water discharge, width, etc., and precisely because of this, the *BI* is very sensitive to changes in the resolution at which the system is analyzed; higher resolution images would reveal finer-scale channels and thus higher *BI*. Despite these significant limitations, *BI* is widely used partly due to its simplicity in computation and interpretation.

We proposed a modification of the *BI* which accounts not only for the count but also for the heterogeneity of channels in multi-thread river systems. We augmented the information content of each cross section using an entropy metric that quantifies the diversity of channels (in terms of flow, channel width or any other relevant property) in each cross section. We defined an entropic *BI* (*eBI*) and interpreted it as the number of effective channels per cross-section, allowing a direct comparison with the traditional *BI*, and the gain of insightful information from the ratio of the two indices.

We showed via analysis of synthetic examples and field and numerical cases that *eBI* contains much more information about the system complexity than *BI*, being at the same time a more robust metric than *BI* as incorporating significantly narrower channels (e.g., due to increasing observational resolution) does not dramatically change *eBI* statistics. In addition, we proposed that interrogating cross-sections in terms of the value *BI/eBI* has the potential to: (a) quantify channel disparity (e.g., in terms of width, water discharge or sediment transport capacity) per cross-section (ii) differentiate braided and anastomosed systems; and (iii) provide information about river cross-section stability to forcing (e.g., seasonal flooding).

Thus, the characterization of multi-thread channel patterns in terms of the effective number of channels (*eBI*) provides not only a most robust quantification but opens up new possibilities to unveil previously hidden relationships. For example, the recent work of Dong and Goudge (2022) showcases how *eBI* allows to interpret and identify river channel patterns from the ancient rock record.

Data Availability Statement

The Global River Widths from Landsat database (Allen & Pavelsky, 2018) is publicly available https://doi.org/10.5281/zenodo.1297434. The Indus water mask used in our analysis can be found in https://esurf.copernicus.org/articles/8/87/2020/esurf-8-87-2020-supplement.zip. The model data used is available at: https://doi.org/10.5281/zenodo.6983538. The software used for the analysis, RivGraph (Schwenk & Hariharan, 2021), is available at https://zenodo.org/record/4591559#.Yo1LIajMKUk.

Acknowledgments

E.F.G. L.V., and A.T. received partial support from NSF Grants EAR-1811909, DMS-1839336, and the UK Research and Innovation Global Challenges Research Fund Living Deltas Hub Grant NES0089261. Moreover, L.Vulis was supported under the NASA Earth and Space Science Fellowship Program Grant 0NSSC18K1409 and the UC-National Lab In-Residence Graduate Fellowship Grant L21GF3569. JS was supported by the Laboratory Directed Research and Development program of Los Alamos National Laboratory under project number 20170668PRD1. The authors want to thank the editor, T.Y. Dong, E.R. Bamber and a third anonymous reviewer for their valuable feedback on improving the manuscript.

References

Allen, G. H., & Pavelsky, T. M. (2018). Global extent of rivers and streams. *Science*, *361*(6402), 585–588. https://doi.org/10.1126/science.aat0636

Ashmore, P. E. (2007). Laboratory modelling of gravel braided stream morphology. *Earth Surface Processes and Landforms*, *7*(3), 201–225. https://doi.org/10.1002/esp.3290070301

Braat, L., Van Kessel, T., Leuven, J. R. F. W., & Kleinhans, M. G. (2017). Effects of mud supply on large-scale estuary morphology and development over centuries to millennia. *Earth Surface Dynamics*, *5*(4), 617–652. https://doi.org/10.5194/esurf-5-617-2017

Carling, P., Jansen, J., & Meshkova, L. (2014). Multichannel rivers: Their definition and classification. *Earth Surface Processes and Landforms*, *39*(1), 26–37. https://doi.org/10.1002/esp.3419

Cover, T. M., & Thomas, J. A. (2006). Elements of information theory. In *Elements of information theory* (2nd ed.). John Wiley and Sons Inc.

Dong, T. Y., & Goudge, T. A. (2022). Quantitative relationships between river and channel-belt planform patterns. *Geology*. https://doi.org/10.1130/g49935.1

Dong, T. Y., Nittrouer, J. A., Mcelroy, B., Il'icheva, E., Pavlov, M., Ma, H., et al. (2020). Predicting water and sediment partitioning in a delta 1 channel network under varying discharge conditions. *Water Resources Research*, *56*(11), e2020WR027199. https://doi.org/10.1029/2020WR027199

Eaton, B. C., Millar, R. G., & Davidson, S. (2010). Channel patterns: Braided, anabranching, and single-thread. *Geomorphology*, *120*(3–4), 353–364. https://doi.org/10.1016/j.geomorph.2010.04.010

Egozi, R., & Ashmore, P. (2008). Defining and measuring braiding intensity. *Earth Surface Processes and Landforms*, *33*(14), 2121–2138. https://doi.org/10.1002/esp.1658

Egozi, R., & Ashmore, P. (2009). Experimental analysis of braided channel pattern response to increased discharge. *Journal of Geophysical Research*, *114*, F02012. https://doi.org/10.1029/2008JF001099

Fahnestock, R. K. (1963). *Morphology and hydrology of a glacial stream -- White River*, Mount Rainier. Survey Professional Paper 422–A. https://doi.org/10.3133/pp422A

Feng, X., Porporato, A., & Rodriguez-Iturbe, I. (2013). Changes in rainfall seasonality in the tropics. *Nature Climate Change*, *3*(9), 811–815. https://doi.org/10.1038/nclimate1907

Fiorentino, M., Claps, P., & Sinoh, V. P. (1993). An entropy-based morphological analysis of river basin networks. In *Water resources research* (Vol. 29).

Foufoula-Georgiou, E., & Sapozhnikov, V. (2001). Scale invariances in the morphology and evolution of braided rivers. *Mathematical Geology*, *33*(3), 273–291. https://doi.org/10.1023/A:1007682005786

Gaurav, K., Métivier, F., Devauchelle, O., Sinha, R., Chauvet, H., Houssais, M., & Bouquerel, H. (2015). Morphology of the Kosi megafan channels. *Earth Surface Dynamics*, *3*(3), 321–331. https://doi.org/10.5194/esurf-3-321-2015

Gong, W., Gupta, H. V., Yang, D., Sricharan, K., & Hero, A. O. (2013). Estimating epistemic and aleatory uncertainties during hydrologic modeling: An information theoretic approach. *Water Resources Research*, *49*(4), 2253–2273. https://doi.org/10.1002/wrcr.20161

Goodwell, A. E., & Kumar, P. (2017). Temporal information partitioning: Characterizing synergy, uniqueness, and redundancy in interacting environmental variables. *Water Resources Research*, *53*(7), 5920–5942. https://doi.org/10.1002/2016WR020216

Hariharan, J., Piliouras, A., Schwenk, J., & Passalacqua, P. (2022). Width-based discharge partitioning in distributary networks: How right we are. *Geophysical Research Letters*, *49*(14). https://doi.org/10.1029/2022GL097897

Huang, H. Q., & Nanson, G. C. (2007). Why some alluvial rivers develop an anabranching pattern. *Water Resources Research*, *43*(7). https://doi.org/10.1029/2006WR005223

Kleinhans, M. G., de Vries, B., Braat, L., & van Oorschot, M. (2018). Living landscapes: Muddy and vegetated floodplain effects on fluvial pattern in an incised river. *Earth Surface Processes and Landforms*, *43*(14), 2948–2963. https://doi.org/10.1002/esp.4437

Kleinhans, M. G., & van den Berg, J. H. (2011). River channel and bar patterns explained and predicted by an empirical and a physics-based method. *Earth Surface Processes and Landforms*, *36*(6), 721–738. https://doi.org/10.1002/esp.2090

Leopold, L. B., & Wolman, M. G. (1957). In *River channel patterns-braided, meandering and straight* (Vol. 282B, pp. 29–85). US Geological Survey Professional Paper.

Limaye, A. B. (2017). Extraction of multithread channel networks with a reduced-complexity flow model. *Journal of Geophysical Research: Earth Surface*, *122*, 1972–1990. https://doi.org/10.1002/2016JF004175

Limaye, A. B., Grimaud, J. L., Lai, S. Y. J., Foreman, B. Z., Komatsu, Y., & Paola, C. (2018). Geometry and dynamics of braided channels and bars under experimental density currents. *Sedimentology*, *65*(6), 1947–1972. https://doi.org/10.1111/sed.12453

Marra, W. A., Kleinhans, M. G., & Addink, E. A. (2014). Network concepts to describe channel importance and change in multichannel systems: Test results for the Jamuna River, Bangladesh. *Earth Surface Processes and Landforms*, *39*(6), 766–778. https://doi.org/10.1002/esp.3482

Meshkova, L. V., & Carling, P. A. (2013). Discrimination of alluvial and mixed bedrock-alluvial multichannel river networks. *Earth Surface Processes and Landforms*, *38*(11), 1299–1316. https://doi.org/10.1002/esp.3417

Nearing, G. S., & Gupta, H. V. (2015). The quantity and quality of information in hydrologic models. *Water Resources Research*, *51*(1), 524–538. https://doi.org/10.1002/2014WR015895

Nicholas, A. (2013). Morphodynamic diversity of the world's largest rivers. *Geology*, *41*(4), 475–478. https://doi.org/10.1130/G34016.1

Porporato, A., & Rodriguez-Iturbe, I. (2013). From random variability to ordered structures: A search for general synthesis in ecohydrology. *Ecohydrology*, *6*(3), 333–342. https://doi.org/10.1002/eco.1400

Ranjbar, S., & Singh, A. (2020). Entropy and intermittency of river bed elevation fluctuations. *Journal of Geophysical Research: Earth Surface*, *125*, e2019JF005499. https://doi.org/10.1029/2019JF005499

Ruddell, B. L., & Kumar, P. (2009a). Ecohydrologic process networks: 1. Identification. *Water Resources Research*, *45*, e2019JF005499. https://doi.org/10.1029/2008WR007279

Ruddell, B. L., & Kumar, P. (2009b). Ecohydrologic process networks: 2. Analysis and characterization. *Water Resources Research*, *45*, W03420. https://doi.org/10.1029/2008WR007280

Sapozhnikov, V. B., & Foufoula-Georgiou, E. (1999). Horizontal and vertical self-organization of braided rivers toward a critical state. *Water Resources Research*, *35*(3), 843–851. https://doi.org/10.1029/98WR02744

Sapozhnikov, V. B., Murray, A. B., Paola, C., & Foufoula-Georgiou, E. (1998). Validation of braided-stream models: Spatial state-space plots, self-affine scaling, and island shapes. *Water Resources Research*, *34*(9), 2353–2364. https://doi.org/10.1029/98WR01697

Schwenk, J., & Hariharan, J. (2021). RivGraph: Automatic extraction and analysis of river and delta channel network topology. *Journal of Open Source Software*, *6*(59), 2952. https://doi.org/10.21105/joss.02952

Schwenk, J., Piliouras, A., & Rowland, J. C. (2020). Determining flow directions in river channel networks using planform morphology and topology. *Earth Surface Dynamics*, *8*(1), 87–102. https://doi.org/10.5194/esurf-8-87-2020

Shannon, C. E. (1948). A mathematical theory of communication. *The Bell system Technical Journal*, *27*(4), 623–656. https://doi.org/10.1002/j.1538-7305.1948.tb00917.x

Singh, V. P. (1997). In *The use of entropy in hydrology and water resources* (Vol. 11). https://doi.org/10.1002/(SICI)1099-1085(199705)11:6⟨587::AID-HYP479⟩3.0.CO;2-P

Tejedor, A., Longjas, A., Caldwell, R., Edmonds, D. A., Zaliapin, I., & Foufoula-Georgiou, E. (2016). Quantifying the signature of sediment composition on the topologic and dynamic complexity of river delta channel networks and inferences toward delta classification. *Geophysical Research Letters*, *43*(7), 3280–3287. https://doi.org/10.1002/2016GL068210

Tejedor, A., Longjas, A., Edmonds, D. A., Zaliapin, I., Georgiou, T. T., Rinaldo, A., & Foufoula-Georgiou, E. (2017). Entropy and optimality in river deltas. *Proceedings of the National Academy of Sciences of the United States of America*, *114*(44), 11651–11656. https://doi.org/10.1073/pnas.1708404114

Tejedor, A., Longjas, A., Passalacqua, P., Moreno, Y., & Foufoula-Georgiou, E. (2018). Multiplex networks: A framework for studying multiprocess multiscale connectivity via coupled-network theory with an application to river deltas. *Geophysical Research Letters*, *45*(18), 9681–9689. https://doi.org/10.1029/2018GL078355

Tejedor, A., Longjas, A., Zaliapin, I., & Foufoula-Georgiou, E. (2015a). Delta channel networks: 1. A graph-theoretic approach for studying connectivity and steady state transport on deltaic surfaces. *Water Resources Research*, *51*(6), 3998–4018. https://doi.org/10.1002/2014WR016577
Tejedor, A., Longjas, A., Zaliapin, I., & Foufoula-Georgiou, E. (2015b). Delta channel networks: 2. Metrics of topologic and dynamic complexity for delta comparison, physical inference, and vulnerability assessment. *Water Resources Research*, *51*(6), 4019–4045. https://doi.org/10.1002/2014WR016604
van Oorschot, M., Kleinhans, M. G., Geerling, G. W., Egger, G., Leuven, R. S. E. W., & Middelkoop, H. (2017). Modeling invasive alien plant species in river systems: Interaction with native ecosystem engineers and effects on hydro-morphodynamic processes. *Water Resources Research*, *53*(8), 6945–6969. https://doi.org/10.1002/2017WR020854